J. Chem. Thermodynamics 43 (2011) 1515–1524

Contents lists available at ScienceDirect

J. Chem. Thermodynamics

journal homepage: www.elsevier.com/locate/jct

Thermodynamic investigation of the (LiF + NaF + CaF_2 + LaF_3) system

M. Beilmann [a,b,*], O. Beneš [a], R.J.M. Konings [a], Th. Fanghänel [a,b]

[a] European Commission, Joint Research Centre, Institute for Transuranium Elements, P.O. Box 2340, 76125 Karlsruhe, Germany
[b] Physikalisch-Chemisches Institut, Ruprecht-Karls-Universitt Heidelberg, Im Neuenheimer Feld 253, 69120 Heidelberg, Germany

ARTICLE INFO

Article history:
Received 15 December 2010
Received in revised form 28 April 2011
Accepted 2 May 2011
Available online 9 May 2011

Keywords:
Molten salts
Phase diagram
Differential scanning calorimetry
Thermodynamics

ABSTRACT

In this work a thermodynamic assessment of the (LiF + NaF + CaF_2 + LaF_3) system is reported. For the thermodynamic modeling of the liquid phase, the classical polynomial model, and the modified quasi-chemical model were used in parallel and compared. The extrapolation to higher order systems was done according to the Toop mathematical formalism. Furthermore, differential-scanning calorimetry data of the ternary (LiF + CaF_2 + LaF_3), (NaF + CaF_2 + LaF_3), and the quaternary (LiF + NaF + CaF_2 + LaF_3) mixtures are presented. Good agreement between the experimental data and the thermodynamic assessment was obtained.

1. Introduction

Fluoride salts are useful for different industrial applications such as extractive metallurgy or electrochemical processes. Other intensive research projects concentrate on the use of molten fluoride salt systems for energy production. Here especially, the development of a molten salt reactor (MSR) has a relatively long history. The MSR belongs to the Generation IV Initiative and several fuel concepts based on fluoride systems exist for this reactor type. Moreover, it was also proposed to use fluoride salts for the energy storage and transfer in solar power towers [1].

For every application information about the thermodynamic properties of the salt systems is necessary. A strong tool can be found in the assessment of phase diagrams. This method is based on the Gibbs free energy minimization between the different phases. With a good description of the phase diagram it is also possible to predict some properties, *e.g.* vapor pressure, for which no experimental information is available.

In this study we perform a full thermodynamic description of the (LiF + NaF + CaF_2 + LaF_3) system in order to collect new data which could be useful for further developments of molten salt reactor designs. In the present case LaF_3 serves as a proxy compound to PuF_3 (AnF_3) as already demonstrated in earlier studies [2], since the direct use of PuF_3 would cause tremendous experimental restrictions. To develop a thermodynamic database first the binary sub-systems are assessed and the higher order systems are extrapolated according to the Toop [3] formalism. For the mathematical description of the excess Gibbs free energy of the liquid solution two thermodynamic models have been used, the classical polynomial formalism and the quasi-chemical model modified by Chartrand and Pelton [4,5].

The main purpose of this study is to compare both approaches, mainly to investigate which one leads to better approximation of higher order systems and to see if the "simple" model (polynomial formalism) has similar accuracy as the more advanced model (quasi-chemical model). In order to make this comparison the melting temperature of several compositions of the (LiF + CaF_2 + LaF_3), (NaF + CaF_2 + LaF_3), and (LiF + NaF + CaF_2 + LaF_3) systems are investigated using the differential-scanning-calorimetry and the results are correlated with our thermodynamic description of the liquid phase.

2. Experimental setup

The sample preparation was done by direct mixing of pure compounds (LiF, NaF, CaF_2, LaF_3) all purchased from Alfar Aesar. Since fluorides are hygroscopic they were stored in a dry glove box with a protection argon atmosphere in which the water content does not exceed a mole fraction of $5 \cdot 10^{-5}$. Before the measurement all salts were dried at a temperature of 423 K for 3 h under a continuous argon flow to lose traces of possibly absorbed water. To minimize the composition error of the examined mixture the initial amount of each pure fluoride salt was filled directly into a DSC crucible. The used crucible consists of a stainless steel body with a inserted boron nitride liner and was developed in the Institute for Transuranium Elements to measure the phase diagrams of fluoride systems as described in detail by Beneš *et al.* [6]. The use of

* Corresponding author at: European Commission, Joint Research Centre, Institute for Transuranium Elements, P.O. Box 2340, 76125 Karlsruhe, Germany. Tel.: +49 7247 951 416; fax: +49 7247 951 99416.
E-mail address: markus.beilmann@ec.europa.eu (M. Beilmann).

0021-9614/$ - see front matter © 2011 Elsevier Ltd. All rights reserved.
doi:10.1016/j.jct.2011.05.002

this crucible is not only necessary to make sure that the salt comes only in contact with inert materials such as boron nitride and nickel, but also to avoid any loss of material by vaporization.

The prepared capsules with the different salt compositions were measured with a Setaram Multi Detector High Temperature Calorimeter (MHTC) using a DSC detector which consists of series of S-type thermocouples. Prior to the measurement a temperature calibration was done using several standard calibration metals (In, Sn, Pb, Zn, Al, Ag, and Au) with known melting temperatures. An empty stainless steel crucible was used as reference to achieve a smooth heat flow signal between this crucible and the sample crucible. The temperature program for all measured compositions consisted of three heating and cooling sequences in the temperature range from (573 to 1273) K. Before each measurement the sample was heated to T = 1273 K and kept there for 1 h to achieve good mixing of the different salt components. After cooling to a temperature of 573 K and stabilizing for another 1 h the sample was heated to T = 1273 K with a heating rate of 3 K/min and cooled back to T = 573 K at 7 K/min. This stabilizing/heating/cooling sequence was repeated again two times.

Due to the supercooling effect of the salt mixtures all transition points were evaluated taking into account only the results from the heating sequence. Since every sample was measured three times we had a good control mechanism to check whether the mixing process was completed. Hence, only if the signals of the different runs were within the experimental error of the device (±2 K) were they taken into account for the final result.

The evaluation of the measured DSC signals was done by determination of the onset point for the eutectic or pertectic temperatures and by the end of the signal for the liquidus temperatures. The evaluation of the signal obtained for the first composition in table 7 is shown in figure 1.

3. Thermodynamic modeling

3.1. Pure compounds and solid solution phases

The mathematical description of a temperature–composition (T–x) phase diagram is very useful to predict various thermodynamic properties of a system even if only few experimental data are available. To determine a T–x phase diagram all existing compounds and phases must be identified and their Gibbs free energy functions must be known. It is very often the case that some of these functions are not available and it is a goal of a thermodynamic assessment to estimate these missing data. During the phase diagram assessment the missing Gibbs free energies are optimized so the best possible fit between the experimental data, *e.g.* solidus and liquidus points and calculated data is obtained.

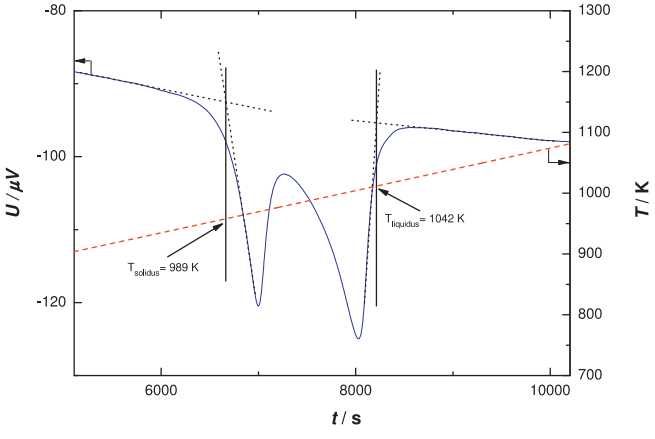

FIGURE 1. Evaluation of a typical melting sequence measured by DSC. U denotes the heat flow signal. To determine the temperature the intercept point between a tangent on the baseline and a tangent on inflection point of the peak is evaluated.

For the pure compounds the Gibbs free energy is defined as:

$$G(T) = H(T) - S(T)\cdot T, \tag{1}$$

where $H(T)$ is the enthalpy and $S(T)$ the entropy, both expressed as functions of the temperature. Since both enthalpy and entropy contributions can be calculated knowing the temperature function of the heat capacity at constant pressure, equation (1) can be written as:

$$G(T) = \Delta_f H^{\circ}_{298.15\,\mathrm{K}} + \int_{298.15\,\mathrm{K}}^{T} C_p dT - T\left(S^{\circ}_{298.15\,\mathrm{K}} + \int_{298.15\,\mathrm{K}}^{T} \frac{C_p}{T} dT\right). \tag{2}$$

The thermodynamic data of all compounds used in this study are summarized in table 1.

The Gibbs free energy function of a solution phase is calculated from the Gibbs free energy of the pure end-members weighted by their mole fractions and a mixing term which is divided into an ideal mixing term and the excess Gibbs free energy term. The general formula for the Gibbs free energy function of a binary (A–B) solution is given below:

$$G(T) = x_A G_A(T) + x_B G_B(T) + RT(x_A \ln x_A + x_B \ln x_B) + G^{xs}, \tag{3}$$

where x_A and x_B are mole fractions of the A and B end-members, respectively, R is the gas constant and G^{xs} is the excess Gibbs free energy.

During the thermodynamic modeling the determination of this excess Gibbs free energy is the main goal and for its description several mathematical models have been developed.

In this work all solid solutions are described using the classical polynomial model in which the excess Gibbs free energy is defined as:

$$G^{xs} = \sum_{ij} x_1 x_2 L_{i,j}, \tag{4}$$

where x_1 and x_2 are the mole fractions of the pure end-members. The term $L_{i,j}$ can be described with the general equation

$$L_{i,j} = a + bT + cT\ln T + dT^2 \cdots, \tag{5}$$

where the parameters $(a, b, \ldots)$ are subject of the optimization during the thermodynamic assessment.

3.2. Liquid solution

The description of the liquid phase is done with the classical polynomial model (described in the previous section) as well as with the quasi-chemical model which was modified according to Chartrand and Pelton [4,5]. In the latter model the key parameter $g_{AB/F}$ is the energy of the second nearest neighbor (SNN) pair exchange reaction in the binary (AF + BF) system:

$$(A{-}F{-}A) + (B{-}F{-}B) = 2(A{-}F{-}B)$$

and can be expressed as a polynomial such as:

$$\Delta g_{AB/F} = \Delta g^{\circ}_{AB/F} + \sum_{(i+j)\geqslant q1} g^{ij}_{AB/F} \chi^{i}_{AB/F} \chi^{j}_{BA/F}. \tag{6}$$

The composition independent coefficients $g^{\circ}_{AB/F}$ and $g^{ij}_{AB/F}$ of this equation are adjusted during the assessment of the binary system. $\chi^{i}_{AB/F}$ and $\chi^{j}_{BA/F}$ are composition variables and depend on the cation–cation pair mole fractions.

$$\chi_{AB/F} = \frac{X_{AA}}{X_{AA} + X_{AB} + X_{BB}}. \tag{7}$$

TABLE 1
$\Delta_f H^\circ$ (298.15 K), S° (298.15 K) and C_p data of the condensed phases of the end-members and the intermediate compounds. $C_p/(\mathrm{kJ}\cdot\mathrm{K}^{-1}\cdot\mathrm{mol}^{-1}) = a + b(T/\mathrm{K}) + c(T^2/\mathrm{K}^2) + d(T^{-2}/\mathrm{K}^{-2})$.

Compound	$\Delta_f H^\circ_{(298.15\,\mathrm{K})}/(\mathrm{kJ}\cdot\mathrm{mol}^{-1})$	$S^\circ_{(298.15\,\mathrm{K})}/(\mathrm{J/K}^{-1}\cdot\mathrm{mol}^{-1})$	a	b	c	d	Reference
LiF(l)	−598.654	42.96	64.183				[7]
NaF(l)	−557.730	52.75	72.989				[7]
CaF_2[a](l)	−1186.0679	92.5655	161.2395	0.0211805		−7683116	[19]
LaF_3(l)	−1633.91975	97.6389266	135				[7]
LiF(cr)	−616.931	35.66	43.31	0.01631	5.04704 E−7	−569124	[7]
NaF(cr)	−576.650	51.21	47.63	0.01479		−464300	[7]
$CaF_2(cr,(s_1))$[b]	−1225.912	68.572	122.8224	0.0284802		−6489901	[19]
$CaF_2(cr,(s_2))$[c]	−1221.142	71.9217	122.8224	0.0284802		−6489901	[19]
LaF_3[d] (cr)	−1669.500	106.98	122.1188	−0.0224674	−1.63094 E−5	−2171380	[e]
$NaLaF_4$(cr)	−2245.5967	161.2	132.61	0.029109	3.4332 E−5	−466070	[f]

[a] T range (298.15 to 1000) K, additional C_p terms $93543.1(T^{-1}/\mathrm{K}^{-1})$, $-5633.815(T^{-0.5}/\mathrm{K}^{-0.5})$. In the T range (1000 to 4000) K $C_p(T)/(\mathrm{kJ}\cdot\mathrm{K}^{-1}\cdot\mathrm{mol}^{-1}) = 99.914$.
[b] A transition between s_1 and s_2 phase occurs at $T = 1424$ K. Additional C_p terms $72535.5(T^{-1}/\mathrm{K}^{-1})$, $-4023.107(T^{-0.5}/\mathrm{K}^{-0.5})$. In the T range (1424 to 2000) K $C_p(T)/(\mathrm{kJ}\cdot\mathrm{K}^{-1}\cdot\mathrm{mol}^{-1}) = 104$.
[c] Additional C_p terms $72535.5(T^{-1}/\mathrm{K}^{-1})$, $-4023.107(T^{-0.5}/\mathrm{K}^{-0.5})$. In the T range (1424 to 2000) K $C_p(T)/(\mathrm{kJ}\cdot\mathrm{K}^{-1}\cdot\mathrm{mol}^{-1}) = 107.989 + 0.01046\ (T/\mathrm{K})$.
[d] Additional $C_p/(\mathrm{kJ}\cdot\mathrm{K}^{-1}\cdot\mathrm{mol}^{-1})$ term $2.81746E{-}8(T^3/\mathrm{K}^3)$.
[e] The C_p function has been taken from the JANAF Tables [7], while the S° (298.15 K) and $\Delta_f H^\circ$(298.15 K) terms have been optimized.
[f] Function derived from the end-members by applying the Neumann-Kopp rule, the S° (298.15 K) and $\Delta_f H^\circ$ (298.15 K) terms optimized in this study.

TABLE 2
Cation–cation coordination numbers of the liquid solutions.

A	B	Z^A_{AB}	Z^B_{AB}
Li^+	Li^+	6	6
Na^+	Na^+	6	6
Ca^{2+}	Ca^{2+}	6	6
La^{3+}	La^{3+}	6	6
Li^+	Na^+	6	6
Li^+	Ca^{2+}	2	6
Na^+	Ca^{2+}	3	6
Li^+	La^{3+}	2	6
Na^+	La^{3+}	2	6
Ca^{2+}	La^{3+}	6	6

An advantage of this model is the possibility to choose the composition of maximum short range ordering in a binary system by setting the ratio of the cation–cation coordination numbers:

$$\frac{Z^A_{AB/FF}}{Z^B_{AB/FF}}. \tag{8}$$

The term $Z^A_{AB/FF}$ for example gives information about how many nearest cationic neighbors of an A atom are B atoms and vice versa. This ratio does not change with composition since it only defines one specific point where the short range ordering shows the strongest effect. This is also a composition where the excess Gibbs free energy tends to have its minimum. The values of the coordination numbers used in this study are summarized in table 2.

In order to keep electroneutrality equation (9) has to be respected. In this equation $q(A)$ and $q(B)$ are the charge numbers of mixing cations A and B, respectively and $q(F)$ is the charge number of the (F^-) anion.

$$\frac{q(A)}{Z^A_{AB/FF}} + \frac{q(B)}{Z^B_{AB/FF}} = \frac{2q(F)}{Z^F_{AB/FF}}. \tag{9}$$

4. Results

A good description of the binary systems builds the basis for the extrapolation to higher order systems. Therefore a critical evaluation of the available literature is needed in order to choose the right datasets which are used to optimize the excess Gibbs free energy parameters. All binary and ternary excess parameters of the liquid phases optimized in this study are summarized in tables 3 and 4. Table 3 shows the data obtained using the classical polynomial model, whereas the values obtained using the quasi-chemical model are given in table 4. The parameters used for the solid solutions are reported in table 5. Furthermore the invariant equilibrium points of all systems are listed in table 6. All thermodynamic calculations in this study were done using the FactSage software [8].

4.1. Binary systems

4.1.1. (CaF_2–LaF_3)

This system was experimentally investigated by Švantner et al. [9] and Ippolitov et al. [10]. Both of them reported a simple eutectic system with large ranges of solid solubility on both sides as shown in figure 2. There are small differences in the eutectic coordinates and for the optimization of the excess Gibbs free energy

TABLE 3
The excess Gibbs free energy parameters of the binary and ternary liquid solutions using the classical polynomial model.

Binary system	$G^{xs}(T)/(\mathrm{J}\cdot\mathrm{mol}^{-1})$	Reference
(LiF + NaF)	$x_{LiF}x_{NaF} - 7384 + 1.81T$	[30]
(LiF + CaF_2)	$x_{CaF_2}x_{LiF}(-5400 + 4.1T) + x^2_{CaF_2}x_{LiF}(-800 - 1T)$	This study
(NaF + CaF_2)	$x_{NaF}x_{CaF_2}(-21304 + 14T) + x^2_{NaF}x_{CaF_2}(2400 + -5T) + x_{NaF}x^2_{CaF_2}(1000 - 2T)$	This study
(LiF + LaF_3)	$x_{LiF}x_{LaF_3}(-11978.2 + -1.5T)$	This study
(NaF + LaF_3)	$x_{NaF}x_{LaF_3}(-34538 - 10.06T) + x^2_{NaF}x_{LaF_3}(-13200 + 12T) + x_{NaF}x^2_{LaF_3}(8000 + 10T)$	This study
(CaF_2 + LaF_3)	$x_{CaF_2}x_{LaF_3}(9500 - 6T) + x^2_{CaF_2}x_{LaF_3}(37863 - 26T) + x_{CaF_2}x^2_{LaF_3}(-8000 - 2T)$	This study
(LiF + NaF + LaF_3)	$x_{LiF}x_{CaF_2}x_{LaF_3}(-10000)$	This study
(LiF + CaF_2 + LaF_3)	$x_{CaF_2}x_{LiF}x_{LaF_3} - 20000 + x^2_{CaF_2}x_{LiF}x_{LaF_3} - 70000 + x_{CaF_2}x_{LiF}x^2_{LaF_3} - 90000$	This study
(NaF + CaF_2 + LaF_3)	$x^2_{NaF}x_{CaF_2}x_{LaF_3}50000 + x_{NaF}x^2_{CaF_2}x_{LaF_3}(-80000)$	This study

TABLE 4
The excess Gibbs free energy parameters of the binary and ternary liquid solutions using the quasi-chemical model.

Binary system	$G^{xs}/(\mathrm{J}\cdot\mathrm{mol}^{-1})$	Reference
(LiF + NaF)	$\Delta g_{\mathrm{LiNa/F}} = 2307 + 0.428T$	[33]
($LiF + CaF_2$)	$\Delta g_{\mathrm{LiCa/F}} = -2183.5 + 1.3591T + 595.7_{\mathrm{LiCa}} - 790.8_{\mathrm{CaLi}}$	[19]
($NaF + CaF_2$)	$\Delta g_{\mathrm{NaCa/F}} = -4266.1 + 2.6451T - 2863.4_{\mathrm{NaCa}} + (-11746.5 + 6.4326T)_{\mathrm{CaNa}}$	[19]
($LiF + LaF_3$)	$\Delta g_{\mathrm{LiLa/F}} = -3712 - 0.620T - 7872_{\mathrm{LaLi}}$	[30]
($NaF + LaF_3$)	$\Delta g_{\mathrm{NaLa/F}} = -13375 + 0.541T - 14440_{\mathrm{LaNa}} - 580_{\mathrm{NaLa}}$	[30]
($CaF_2 + LaF_3$)	$\Delta g_{\mathrm{CaLa/F}} = (-544 + 0.541T) - 3347.2_{\mathrm{CaLa}} - 4393.2_{\mathrm{LaCa}}$	This study
($LiF + NaF + LaF_3$)	$\Delta g^{001}_{\mathrm{LiNa(La)/FF}} = 9566$	This study
($LiF + CaF_2 + LaF_3$)	$\Delta g^{001}_{\mathrm{CaLa(Li)/FF}} = 1674$	This study
($NaF + CaF_2 + LaF_3$)	$\Delta g^{001}_{\mathrm{CaLa(Na)/FF}} = 16736$	This study

TABLE 5
The excess Gibbs free energy parameters of the binary solid solutions using the classical polynomial model.

Binary system	$G^{xs}(T)/(\mathrm{J}\cdot\mathrm{mol}^{-1})$	Reference
(LiF + NaF)	$x_{\mathrm{LiF}}x_{\mathrm{NaF}}22250 + x^3_{\mathrm{LiF}}x_{\mathrm{NaF}}17250$	[30]
($CaF_2 + LaF_3$)	$x_{\mathrm{CaF_2}}x_{\mathrm{LaF_3}}(37000 + 30.5T)$	This study[a]
($CaF_2 + LaF_3$)	$x_{\mathrm{LaF_3}}x_{\mathrm{CaF_2}}(78000 - 48.5T)$	This study[b]

[a] $G^{\circ}_{\mathrm{LaF_3,cubic}} = G^{\circ}_{\mathrm{LaF_3}} + 10000$ J.
[b] $G^{\circ}_{\mathrm{CaF_2,hexagonal}} = G^{\circ}_{\mathrm{CaF_2}} + 10000$ J.

parameters the dataset of Švantner et al. [9] was preferred because in their work the solid state solubility is much better described.

A maximal solid solubility of 23 mol% of CaF_2 in LaF_3 is found at the eutectic temperature. X-ray analysis showed that this solid solution crystallizes in hexagonal tysonite type structure. At the other side of the phase diagram LaF_3 is soluble up to 46 mol% in CaF_2 crystallizing in fluorite type structure. Since eighter the dissolved CaF_2 or LaF_3 are not in their thermodynamic stable crystal structure in those solid solutions, an arbitrary increase of 10 kJ/mol for the enthalpy of formation was chosen for CaF_2 in the hexagonal structure and for LaF_3 in the fluorite structure. The different excess Gibbs free energy parameters used in the performed optimization of the liquid phase using the classical polynomial model and the quasi-chemical model, respectively are shown in tables 3 and 4. The parameters for the classical polynomial description of the solid solutions can be found in table 5.

4.1.2. $LiF–CaF_2$

In the present study different experimental datasets [11–13] including enthalpies of mixing [14] were used to fit the excess

TABLE 6
Invariant equilibrium points of all phase diagrams related to the ($LiF + NaF + CaF_2 + LaF_3$) system. x is the mole fraction of the respective salt.

System	Equilibrium	Model	$T_{calc.}$/K	x_{LiF}	x_{NaF}	$x_{\mathrm{CaF_2}}$	$x_{\mathrm{LaF_3}}$
(LiF + NaF)	Eutectic	[a]	922	0.606	0.394		
	Eutectic	[b]	920	0.605	0.395		
($LiF + CaF_2$)	Eutectic	[a]	1038	0.796		0.204	
	Eutectic	[b]	1038	0.789		0.211	
($NaF + CaF_2$)	Eutectic	[a]	1089		0.686	0.314	
	Eutectic	[b]	1089		0.672	0.328	
($LiF + LaF_3$)	Eutectic	[a]	1043	0.840			0.160
	Eutectic	[b]	1043	0.833			0.167
($NaF + LaF_3$)	Eutectic	[a]	1008		0.729		0.271
	Peritectic	[a]	1060		0.673		0.327
	Eutectic	[b]	1009		0.717		0.283
	Peritectic	[b]	1058		0.662		0.338
($CaF_2 + LaF_3$)	Eutectic	[a]	1585			0.438	0.562
	Eutectic	[b]	1585			0.445	0.555
($LiF + NaF + CaF_2$)	Eutectic	[a]	884	0.511	0.365	0.124	
	Eutectic	[b]	887	0.520	0.373	0.108	
($LiF + NaF + LaF_3$)	Eutectic	[a]	854	0.419	0.428		0.153
	Peritectic	[a]	869	0.439	0.392		0.169
	Eutectic	[b]	851	0.420	0.436		0.144
	Peritectic	[b]	867	0.442	0.400		0.158
($LiF + CaF_2 + LaF_3$)	Eutectic	[a]	981	0.666		0.176	0.158
	Peritectic	[a]	1002	0.632		0.194	0.174
	Eutectic	[b]	985	0.684		0.177	0.139
	Peritectic	[b]	1002	0.664		0.188	0.148
($NaF + CaF_2 + LaF_3$)	Eutectic	[a]	985		0.677	0.095	0.228
	Peritectic	[a]	1016		0.634	0.108	0.259
	Peritectic	[a]	1029		0.618	0.107	0.275
	Eutectic	[b]	984		0.656	0.104	0.240
	Peritectic	[b]	1014		0.611	0.113	0.276
	Peritectic	[b]	1025		0.599	0.109	0.292
($LiF + NaF + CaF_2 + LaF_3$)	Minimum	[a]	839	0.392	0.388	0.064	0.156
	Minimum	[b]	841	0.406	0.404	0.045	0.145

[a] Classical polynomial model.
[b] Quasi-chemical model.

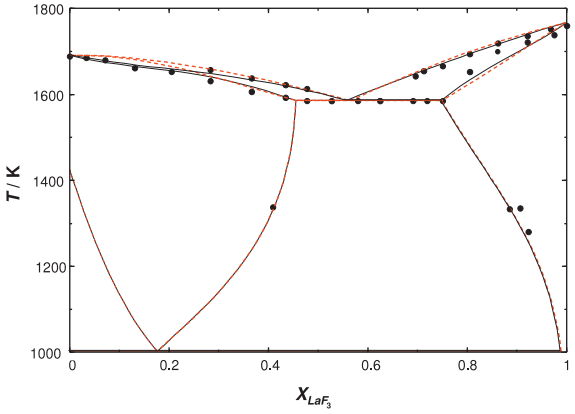

FIGURE 2. Calculated phase diagram of the (CaF_2 + LaF_3) system. The solid line shows the quasi-chemical model and the dashed line the classical polynomial model. (●) Experimental points by Švantner et al. [9].

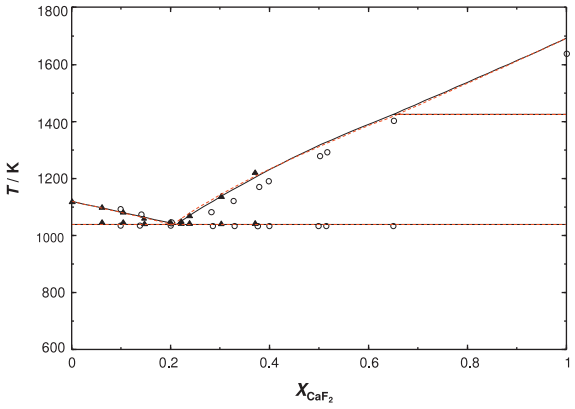

FIGURE 3. Calculated phase diagram of the (LiF + CaF_2) system. The solid line shows the quasi-chemical model and the dashed line the classical polynomial model. (▲) Experimental points by Roake [11]; (○) experimental points by Deadmore and Machin [12].

parameters of the liquid phase of the binary (LiF + CaF_2) system using the classical polynomial model.

The description with the quasi-chemical model was already done by Chartrand *et al.* [19] who based the thermodynamic

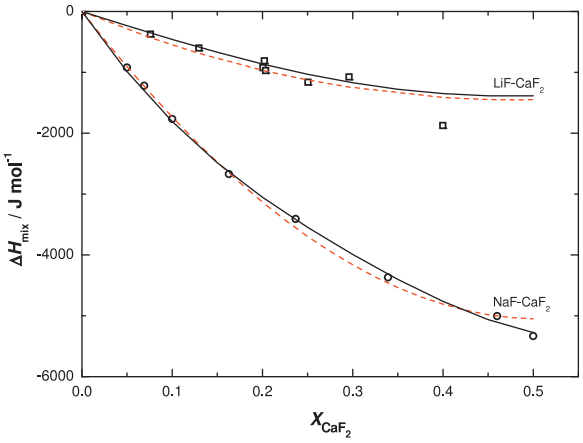

FIGURE 4. Calculated enthalpies of mixing of the (LiF + CaF_2) and (NaF + CaF_2) system. (□) Experimental data for the (LiF + CaF_2) system; (○) experimental data for the (NaF + CaF_2) system. The solid line shows the calculation with the quasi-chemical model and the dashed line shows the classical polynomial model.

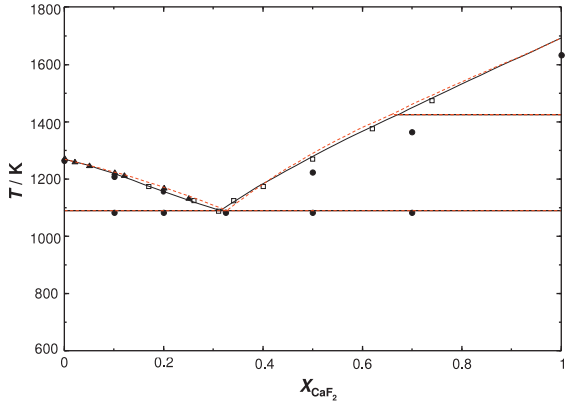

FIGURE 5. Calculated phase diagram of the (NaF + CaF_2) system. The solid line shows the quasi-chemical model and the dashed line the classical polynomial model. (▲) Experimental points by Cantor [21]; (●) by Fedotieff et al. [22]; (□) by Barton et al. [20].

assessment on several measurements [11–18]. In agreement to the work of Chartrand *et al.* a single eutectic system with no solution in the solid state is reported. The calculated phase diagram is shown in figure 3. A comparison of the experimental and calculated enthalpies of mixing is given in figure 4.

4.1.3. NaF–CaF_2

In this work the excess parameters for the description of the liquid phase using the classical polynomial model were obtained by taking into account the experimental data from [20–22] and enthalpies of mixing measured by Hong and Kleppa [14]. The optimization of the (NaF + CaF_2) binary system with the quasi-chemical model was done by the same authors [19] as for the (LiF + CaF_2) system. In agreement with experimental investigations [14,20–23] and our work the authors reported a single eutectic system with no solid solubility. The NaF–CaF_2 phase diagram is shown in figure 5, while figure 4 reports the experimental enthalpies of mixing compared with the calculations.

4.1.4. LiF–LaF_3

The liquid solution thermodynamic assessment of this simple eutectic system, shown in figure 6, was thermodynamically assessed in this work using the classical polynomial model. The

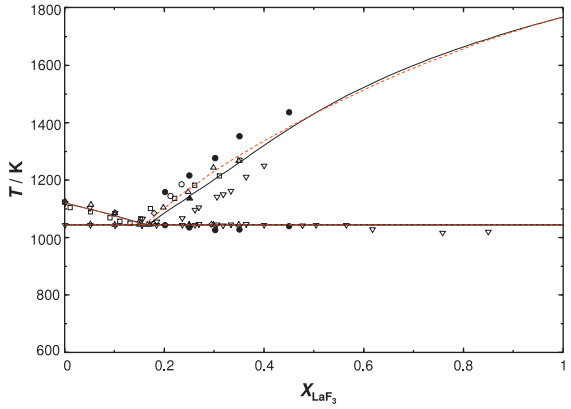

FIGURE 6. Calculated phase diagram of the (LiF + LaF_3) system. The solid line shows the quasi-chemical model and the dashed line the classical polynomial model. (▲) Experimental points by Thoma et al. [27]; (●) by van der Meer et al. [24]; (□) by Bukhalova et al. [25]; (▽) by Khripin [26]; (◇) DTA data by Abdoun et al. [29]; (○) calorimetric data by Abdoun et al. [29]; (△) by Agulyanski and Bessonova [28], last as reference in [29].

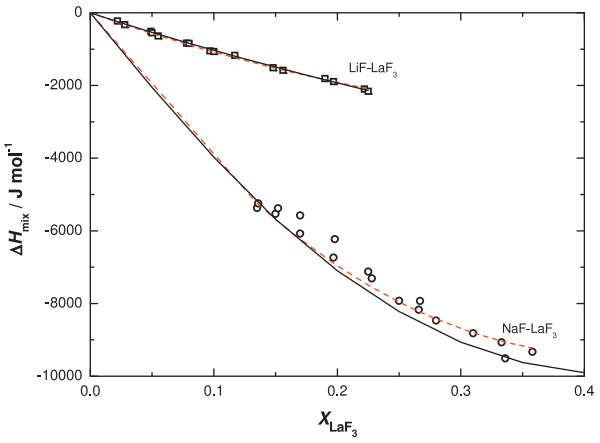

FIGURE 7. Calculated enthalpies of mixing in the (LiF + LaF_3) and (NaF + LaF_3) system. □ Experimental data for the (LiF + LaF_3) system; (○) experimental data for the (NaF + LaF_3) system. The solid line shows the calculation with the quasi-chemical model and the dashed line shows the classical polynomial model.

assessment was based on experimentally obtained equilibrium data [24–28] as well as on enthalpies of mixing [29].

The description with the quasi-chemical model was obtained by Beneš *et al.* [30] based on the same data and is used in the present study without any changes. The comparison between the experimental and calculated enthalpies of mixing is reported in figure 7.

4.1.5. NaF–LaF_3

In this study the (Na, La)F_x liquid solution is described with the classical polynomial model. On the basis of the experimental equilibrium data measured by Abdoun *et al.* [29] and van der Meer *et al.* [24] and experimentally determined enthalpies of mixing measured by Abdoun *et al.* [29] an eutectic ($T = 1008$ K, $x_{LaF_3} = 27.1$ mol%) and a peritectic point ($T = 1060$ K, $x_{LaF_3} = 33.8$ mol%) was found. The $NaLaF_4$ compound is formed in the solid state and decomposes at the peritectic temperature. No evidence for solid solubility was found.

The optimization of the NaF–LaF_3 phase diagram using the quasi chemical model for the liquid phase has been reported by Beneš et al. [30] based on the same dataset. In that study almost identical data were found for the eutectic ($T = 1009$ K, $x_{LaF_3} = 28.3$ mol%) and the peritectic equilibrium ($T = 1058$ K, $x_{LaF_3} = 33.8$ mol%). The phase diagram is shown in figure 8 whereas the calculated

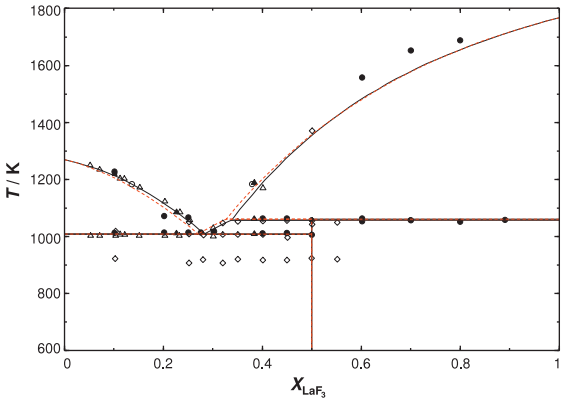

FIGURE 8. Calculated phase diagram of the (NaF + LaF_3) system. The solid line shows the quasi-chemical model and the dashed line the classical polynomial model. (•) Experimental points by van der Meer et al. [24]; (◇) DTA data by Abdoun et al. [29]; (○) calorimetric data by Abdoun et al. [29]; (△) by Matthes and Holz [31]; (▲) by Grande [32] last two as reference in [29].

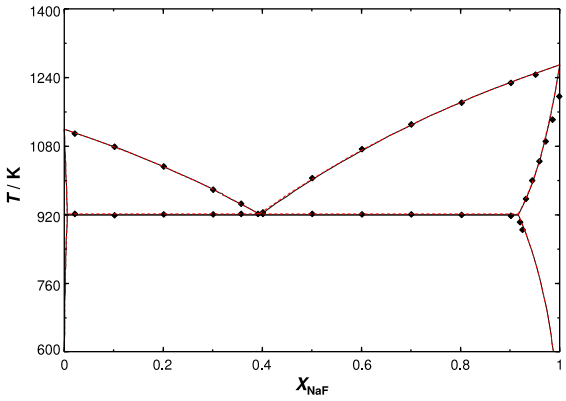

FIGURE 9. Calculated phase diagram of the (LiF + NaF) system. The solid line shows the quasi-chemical model and the dashed line the classical polynomial model. (♦) Experimental points by Holm [34].

enthalpies of mixing are compared with the experimental values in figure 7.

4.1.6. LiF–NaF

The description of the (LiF + NaF) system was already done with both models by Beneš *et al.* [30,33] in two different studies and their data are used in this work without any changes. This system has been reported as a single eutectic system with limited solubility in the solid state at the LiF and NaF side as shown in figure 9. The maximal solubility of the solid state is reached at the eutectic temperature ($T = 921$ K) with 8.3 mol% of LiF diluted in NaF and 0.6 mol% of NaF diluted in LiF. The optimization of this system was based on the experimental equilibrium data taken from Holm [34] and on the mixing enthalpies measured by Hong and Kleppa [14] at $T = 1360$ K. A comparison between the experimental mixing enthalpies and the calculated values using both models is shown in figure 10.

4.2. Ternary systems

4.2.1. LiF–CaF_2–LaF_3

In this study the liquid phase of the (LiF + CaF_2 + LaF_3) system was experimentally investigated with the DSC technique. To our best knowledge no other experimental data are available, thus the optimization with the quasi-chemical model as well as with the classical polynomial model was based only on our own

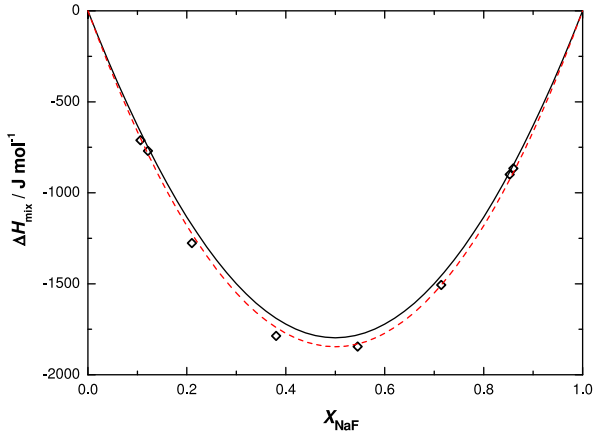

FIGURE 10. Calculated enthalpies of mixing in the (LiF + NaF) system, (◇) experimental data by Kleppa and Hong [14], (solid line) classical polynomial model, (dashed line) quasi-chemical model.

measurements. This system is characterized by one eutectic and one peritectic point as given in figure 11. These invariant equilibria are reported in table 6 for both descriptions. No evidence for ternary solubility in the solid state was found. Table 7 and figure 12 show the obtained experimental values compared with our calculation. A good agreement between the data was obtained in case of both models with an average difference of less than 2%. Also the eutectic temperatures, 981 K and 985 K for the classical polynomial model and the quasi-chemical model respectively, are in good agreement to the experimental value of 989 K.

Out of 11 measured compositions, for two of them (the last two lines in table 7) the liquidus temperature could not be determined. Here an additional signal appeared in the cooling sequences of the DSC measurements which could not be reproduces upon heating. These signals were measured at higher temperatures with much lower intensity than the other signals and could correspond to the calculated liquidus temperatures. This effect is possibly caused by a decrease of the sensitivity using the DSC crucibles as discussed in [6].

4.2.2. NaF–CaF_2–LaF_3

DSC measurements on this system have been performed in this study. Based on the obtained dataset an optimization of the liquid phase was done with both thermodynamic models. Three invariant equilibrium points were found, one eutectic and two peritectics, as shown in figure 13. The exact coordinates are presented in table 6.

Good agreement between the calculation and the experiments was obtained as reported in table 8 and figure 14. Out of 10 measured points only one liquidus temperature deviated from the calculation by more than 2.5%. As shown in table 8 the difference between the two models are negligible, the eutectic temperature differing by only 1 K (classical polynomial model $T = 984$ K and quasi-chemical model $T = 985$ K).

During the measurement of the composition with 60 mol% NaF, 20 mol% CaF_2 and 20 mol% of LaF_3 a much stronger signal in the cooling sequences was observed which was almost not detectable during the heating as demonstrated in figure 15.

The composition for which the experimentally determined temperature has a bigger deviation from the calculations ($x_{NaF} = 0.625$, $x_{CaF_2} = 0.075$ and $x_{LaF_3} = 0.300$) does not show this behavior. The temperature obtained from the experiment seems to be quite high since the corresponding composition in the binary NaF–LaF_3 phase

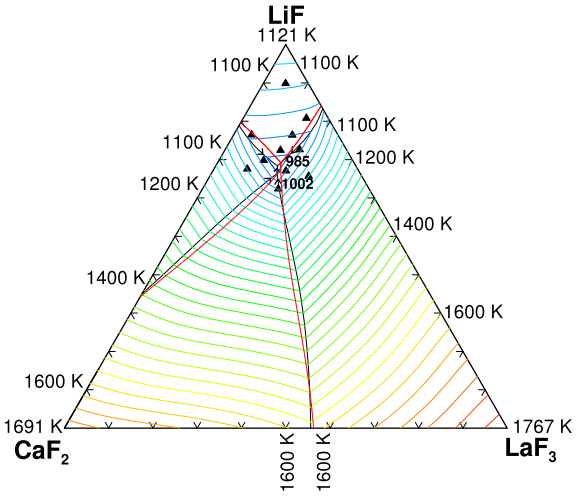

FIGURE 11. Calculated liquid projection of the (LiF + CaF_2 + LaF_3) system with the quasi-chemical model. Isotherms are labeled in K, with an interval of 25 K. The dashed line shows the univariant lines of the classical polynomial model. Experimental data points (▲) are obtained in this study. The experimental and calculated liquidus temperatures can be found in table 7.

TABLE 7
DSC measurements of the (LiF + CaF_2 + LaF_3) system. The data are compared with the calculated temperature using the classical polynomial model and the quasi-chemical model. x is the mole fraction of the respective salt.

x_{LiF}	x_{CaF_2}	x_{LaF_3}	$T^{solidus}_{exp.}$/K	$T^{liquidus}_{exp.}$/K	$T_{calc.}$[a]/K	$T_{calc.}$[b]/K
0.809	0.049	0.142	989	1042	1039	1042
0.699	0.201	0.101	990	1018	1023	1016
0.900	0.051	0.050	990	1091	1081	1082
0.727	0.106	0.168	990	1019	1009	1015
0.765	0.103	0.132	988	1038	1026	1026
0.766	0.195	0.040	989	1039	1027	1031
0.672	0.164	0.165	986	1007	991	1016
0.725	0.150	0.125	993	1013	1011	1010
0.625	0.205	0.170	982	1011	1016	1046
0.677	0.249	0.075	991		1085	1072
0.658	0.120	0.222	987		1080	1092

[a] Classical polynomial model.
[b] Quasi-chemical model.

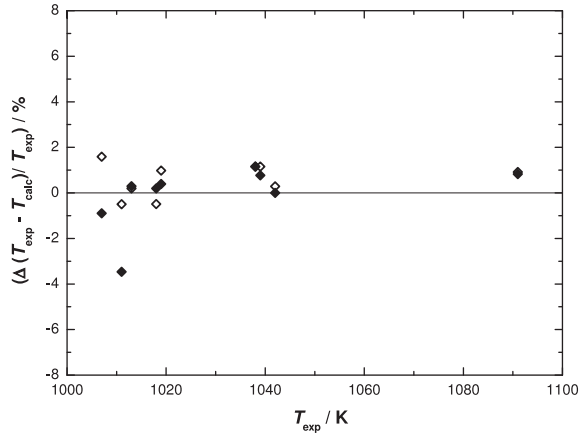

FIGURE 12. Deviation of the calculated melting temperatures from the experimental liquidus temperatures for the (LiF + CaF_2 + LaF_3) system. (♦) deviation using the quasi-chemical model; (◇) Deviation using the classical polynomial model.

diagram with 67.6 mol% NaF and 32.4 mol% of LaF_3 has a calculated liquidus temperature of 1047 K and in the calculated ternary phase diagrams it is not obvious that the addition of 7 mol% of CaF_2 causes an increase of the temperature of nearly 40 K. At this composition the calculations with the two models show an exceptional high difference of 30 K.

4.2.3. LiF–NaF–LaF_3

An optimization of the liquid phase of this system using the quasi-chemical model was published by Beneš *et al.* [30]. In this

TABLE 8
DSC measurements of the (NaF + CaF_2 + LaF_3) system. The data are compared with the calculated temperature using the classical polynomial model and the quasi-chemical model. x is the mole fraction of the respective salt.

x_{NaF}	x_{CaF_2}	x_{LaF_3}	$T^{solidus}_{exp.}$/K	$T^{liquidus}_{exp.}$/K	$T_{calc.}$[a]/K	$T_{calc.}$[b]/K
0.762	0.107	0.131	994	1123	1103	1100
0.661	0.119	0.220	991	1012	1011	1002
0.671	0.254	0.075	996	1072	1066	1064
0.671	0.164	0.165	994	1042	1033	1032
0.700	0.050	0.250	1002	1022	999	1018
0.625	0.075	0.300	999	1085	1056	1026
0.590	0.150	0.260	990	1061	1075	1059
0.600	0.200	0.200	997	1080	1088	1071
0.751	0.049	0.200	1000	1086	1064	1073
0.750	0.175	0.076	993	1114	1117	1108

[a] Classical polynomial model.
[b] Quasi-chemical model.

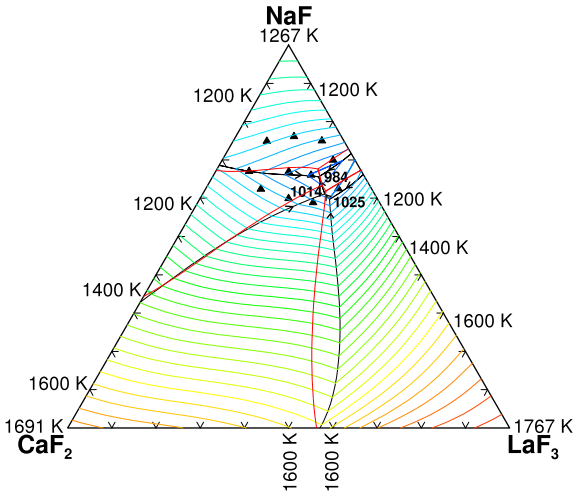

FIGURE 13. Calculated liquid projection of the ($NaF + CaF_2 + LaF_3$) system with the quasi-chemical model. Isotherms are labeled in K, with an interval of 25 K. The dashed line shows the univariant lines of the classical polynomial model. Experimental data points (▲) are obtained in this study. The experimental and calculated liquidus temperatures can be found in table 8.

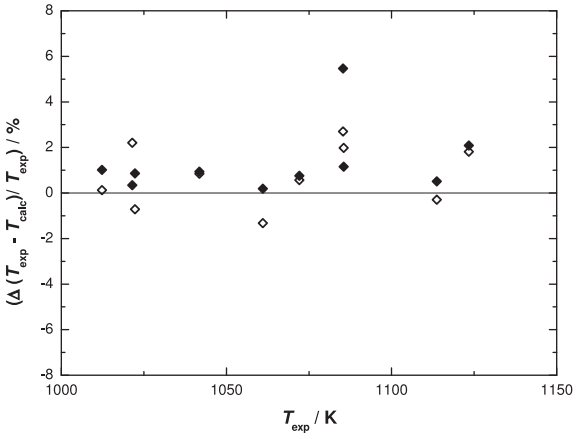

FIGURE 14. Deviation of the calculated melting temperatures from the experimental liquidus temperatures for the ($NaF + CaF_2 + LaF_3$) system. (♦) Deviation using the quasi-chemical model; (◇) deviation using the classical polynomial model.

system one eutectic and one peritectic invariant equilibria were reported and the phase diagram is shown in figure 16.

The description of the liquid solution with the classical polynomial model was performed in this study based on the experimental data by van der Meer *et al.* [24]. These equilibrium points were obtained using the DSC technique. In contrast to the measurements performed in the present study on other fluoride systems the sample preparation in the work of van der Meer *et al.* was not done by direct mixing of the corresponding pure end-members in the measured crucible but mixing the fluoride salts in a mortar. As a consequence of this preparation technique a somewhat larger composition error must be taken into account. Moreover the samples measured by van der Meer *et al.* were not encapsulated during the DSC measurements. At high temperatures a composition shift can occur due to incongruent vaporisation. For example at $T = 1200$ K calculations with the quasi-chemical model for the composition ($x_{LiF} = 0.197$, $x_{NaF} = 0.404$, $x_{LaF_3} = 0.399$) showed a huge difference in the vapor pressure of the end-members. The values for LiF ($p = 2.4$ Pa) and NaF ($p = 1.8$ Pa) are comparable but there is a difference of two orders of magnitude compared to the value of LaF_3 ($p = 2.0 \cdot 10^{-2}$ Pa).

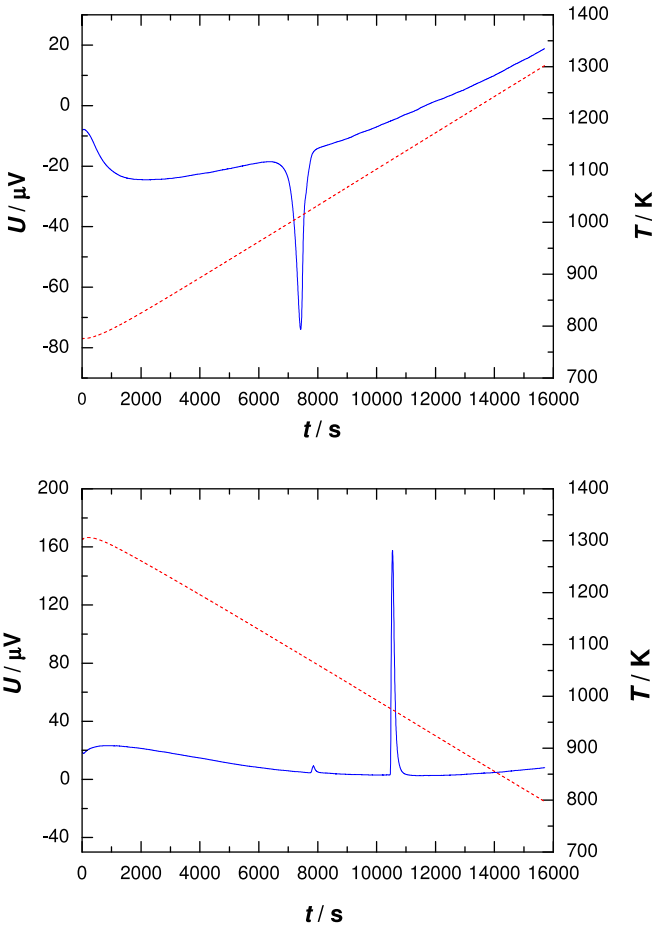

FIGURE 15. Comparison of the heating and cooling sequence in the DSC measurement with the sample composition 60 mol% NaF, 20 mol% CaF_2 and 20 mol% of LaF_3. *U* denotes the heat flow signal. The upper graph shows the heating sequence. The lower graph shows the cooling sequence with an additional signal which was not detected during heating. The dashed line represents the temperature.

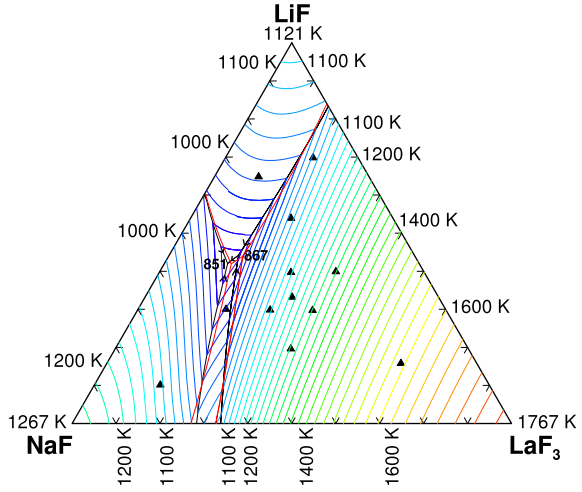

FIGURE 16. The LiF–NaF–LaF_3 phase diagram. Calculated liquid projection of the ($LiF + NaF + LaF_3$) system with the quasi-chemical model. Isotherms are labeled in K, with an interval of 25 K. The dashed line shows the univariant lines of the classical polynomial model. Experimental data points (▲) are taken from van der Meer et al. [24]. The experimental and calculated liquidus temperatures can be found in table 9.

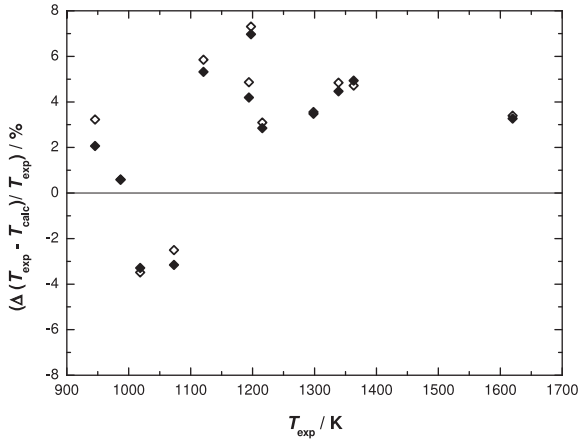

FIGURE 17. Deviation of the calculated melting temperatures from the experimental liquidus temperatures for the (LiF + NaF + LaF_3) system. (♦) Deviation using the quasi-chemical model; (◇) deviation using the classical polynomial model.

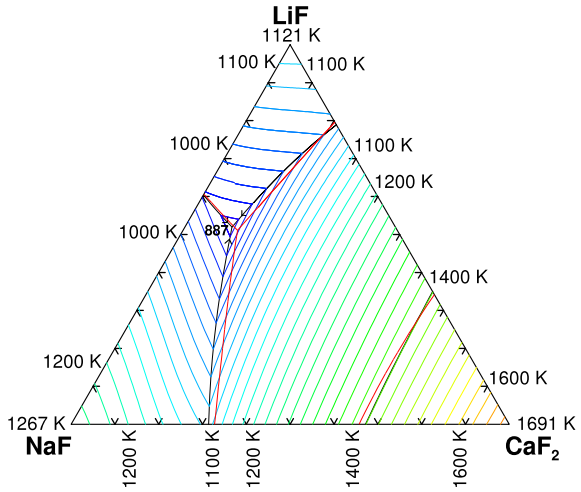

FIGURE 18. The (LiF + NaF + CaF_2) phase diagram. Calculated liquid projection of the (LiF + NaF + CaF_2) system with the quasi-chemical model. Isotherms are labeled in K, with an interval of 25 K. The dashed line shows the univariant lines of the classical polynomial model.

In order to achieve a good agreement between the experimental data and the calculation a small ternary excess Gibbs parameter was used. From the comparison of the calculated phase diagrams and the experimental equilibrium points more than 80% of the data are within 5% error as shown in figure 17, which is acceptable agreement as increased composition error of the measurement can be expected due to the reasons discussed in the previous paragraph. As shown in the phase diagram with the marked experimental investigated compositions in figure 16 the (LiF + NaF + $LaF)_3$ system has a quite sharp liquid phase field where most of the measurements were carried out. In this case a small composition deviation has a strong effect on the liquidus temperature. For example if the discussed experimental point ($x_{LiF} = 0.197$, $x_{NaF} = 0.404$, $x_{LaF_3} = 0.399$) looses only 1 mol% of LiF and NaF the liquidus point increases by about 30 K. This temperature would correspond much better to the experimentally determined melting temperature.

A comparison between all experimental and calculated temperatures is reported in detail in table 9.

4.2.4. LiF–NaF–CaF_2

The liquidus projection of the ternary (LiF + NaF + CaF_2) system has been reported in previous studies [19,20,35]. In all studies a single eutectic system with no solid solubility in the ternary field was found. Relatively good agreement between the corresponding eutectic temperatures 898 K [20], 880 K [35] and 886 K [19] from these sources was found. In the optimization using the quasi-chemical model by Chartrand *et al.* [19] no ternary excess parameters were used.

In this work the liquid phase was assessed with the classical polynomial model and also in this case no ternary excess parameters were needed. The eutectic temperature was found at 884 K compared to 887 K obtained using the quasi-chemical model. The LiF–NaF–CaF_2 phase diagram is shown in figure 18.

4.3. Quaternary system

4.3.1. LiF–NaF–CaF_2–LaF_3

DSC measurements of several compositions of this system have been performed in the present study and the results were compared with the thermodynamic assessments. These measurements were mainly focused on compositions with low LaF_3 concentrations according to the reference fuel composition of the molten salt reactor operating as an actinide burner. In the present case LaF_3 is considered as analog to PuF_3 whereas LiF, NaF and CaF_2 are the solvent components. Thus these results can be used in the future to predict the melting behavior of such kind of fuel.

Since the obtained experimental data are in good agreement with the calculation, no quaternary excess parameters were needed to describe the liquid phase. The description with the

TABLE 9
DSC measurements of the (LiF + NaF + LaF_3) system by van der Meer [24]. The data are compared with the calculated temperature using the classical polynomial model and the quasi-chemical model. *x* is the mole fraction of the respective salt.

x_{LiF}	x_{NaF}	x_{LaF_3}	$T^{liquidus}_{exp.}$/K	$T_{calc.}$[a]/K	$T_{calc.}$[b]/K
0.102	0.748	0.150	1073	1100	1107
0.159	0.172	0.669	1620	1565	1567
0.197	0.404	0.399	1298	1252	1253
0.298	0.304	0.398	1339	1274	1279
0.299	0.400	0.301	1198	1110	1119
0.301	0.499	0.200	946	915	926
0.333	0.333	0.334	1216	1178	1181
0.400	0.200	0.400	1363	1299	1296
0.398	0.303	0.299	1194	1136	1144
0.540	0.232	0.228	1121	1055	1061
0.649	0.251	0.100	987	981	981
0.699	0.102	0.199	1019	1054	1052

[a] Classical polynomial model.
[b] Quasi-chemical model.

TABLE 10
DSC measurements of the (LiF + NaF + CaF_2 + LaF_3) system. The data are compared to the calculated temperature using the classical polynomial model and the quasi-chemical model. *x* is the mole fraction of the respective salt.

x_{LiF}	x_{NaF}	x_{CaF_2}	x_{LaF_3}	$T^{solidus}_{exp.}$/K	$T^{liquidus}_{exp.}$/K	$T_{calc.}$[a]/K	$T_{calc.}$[b]/K
0.526	0.278	0.147	0.049	843	928	947	985
0.501	0.347	0.099	0.059	846	898	892	911
0.607	0.300	0.080	0.013	843	951	942	941
0.523	0.356	0.108	0.013	840	897	894	895
0.523	0.349	0.108	0.020	845	896	896	901
0.650	0.220	0.110	0.020	845	983	971	969
0.522	0.327	0.130	0.021	843	952	910	948
0.490	0.383	0.108	0.020	845	892	891	900
0.408	0.393	0.065	0.134	847	868	853	887

[a] Classical polynomial model.
[b] Quasi-chemical model.

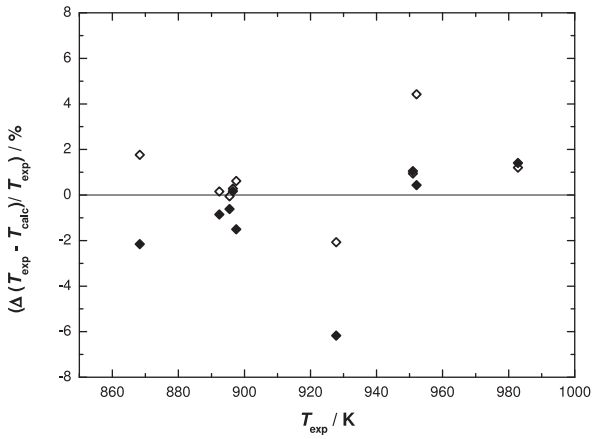

FIGURE 19. Deviation of the calculated melting temperatures from the experimental liquidus temperatures for the (LiF + NaF + CaF_2 + LaF_3) system. (♦) Deviation using the quasi-chemical model; (◇) deviation using the classical polynomial model.

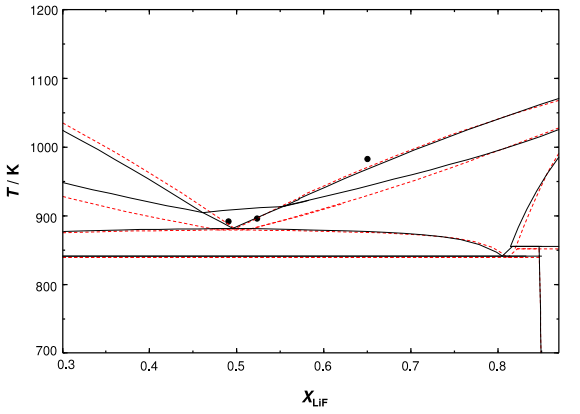

FIGURE 20. Pseudo-binary LiF–NaF phase diagram of the (LiF + NaF + CaF_2 + LaF_3) system. The CaF_2 as well as the LaF_3 content stays constant at $x_{CaF_2} = 0.11$ and $x_{LaF_3} = 0.02$.

classical polynomial model reproduces the experimental values slightly better with an average difference of 1.3% compared to 1.6% from the quasi-chemical model but this difference is marginal, as it falls within the experimental error of the measuring technique used. The exact values are reported in table 10 and figure 19. In figure 20 the pseudo-binary LiF–NaF phase diagram is shown with constant composition values of CaF_2 ($x_{CaF_2} = 11$ mol%) and LaF_3 ($x_{LaF_3} = 2$ mol%) where the good agreement between the two calculations and some experimental values is illustrated.

5. Conclusions

In this work we performed a thermodynamic evaluation of all binary and ternary phase diagrams of the quaternary (LiF + NaF + - CaF_2 + LaF_3) system. The liquid solution was described by the classical polynomial model and the quasi-chemical model, whereas solid solutions were described with the classical polynomial model only.

Based on the optimized binary phase diagrams the higher order systems were extrapolated using the Toop mathematical formalism where CaF_2 and LaF_3 were selected as asymmetric components. The performed DSC measurements of the (LiF + CaF_2 + LaF_3), (NaF + CaF_2 + LaF_3), and (LiF + NaF + CaF_2 + LaF_3) systems served as basis for the optimization of the related liquid phases.

It was shown that with the classical polynomial model as well as the quasi-chemical model we obtained a good agreement with the experimental data, both models showing similar extrapolations to higher order systems.

For the quaternary (LiF + NaF + CaF_2 + LaF_3) system the measurements were done for low LaF_3 concentrations representing typical amounts of PuF_3 (simulated by LaF_3) in the fuel of the molten salt reactor when designed as actinide burner concept. The addition of small amounts of LaF_3 to the (LiF + NaF + CaF_2) system causes only minor differences on the melting temperature compared to the ternary system, and thus the difference between both models for the liquid phase in this region of the quaternary system is not significant. It was also shown in this study that much better agreement between the calculation and the experiment, when investigating the phase equilibrium of the fluoride salts, is achieved using the encapsulation technique as developed in [6].

Acknowledgments

M.B. acknowledges greatfully the support of the European Commission, given in the frame of the programme "Training and Mobility of Researchers". The authors would like to thank Sorin Octavian Valu for the help in performing the measurements.

References

[1] C.W. Forsberg, P.F. Peterson, H. Zhao, J. Solar Energy Eng. (129) (2007) 141–146.
[2] O. Beneš, R.J.M. Konings, J. Nucl. Mater. 377 (3) (2008) 449–457.
[3] A.D. Pelton, Calphad 25 (2001) 319–328.
[4] A.D. Pelton, P. Chartrand, G. Eriksson, Metall. Trans. 32A (2001) 1409–1416.
[5] P. Chartrand, A.D. Pelton, Metall. Trans. 32A (2001) 1397–1407.
[6] O. Beneš, R.J.M. Konings, S. Wurzer, M. Sierig, A. Dockendorf, Thermochim. Acta 509 (1-2) (2010) 62–66.
[7] M.W. Chase, Jr., NIST-JANAF Thermochemical Tables Fourth Edition, J. Phys. Chem. Ref. Data, Monograph 9 (1998).
[8] C.W. Bale et al., FactSage Software v. 5.5.
[9] M. Švantner, E. Mariani, P.P. Fedorov, B.P. Sobolev, Kristall und Technik 14 (3) (1979) 365–369.
[10] E.G. Ippolitov, N.G. Gogadze, B.M. Zhigarnovskii, Russian J. Inorg. Chem. 15 (12) (1970).
[11] W.E. Roake, J. Electrochem. Soc. 104 (1957) 661–662.
[12] D.L. Deadmore, J.S. Machin, J. Phys. Chem. 64 (1960) 824–825.
[13] G.A. Bukhalova, A.G. Bergman, Dokl. Akad. Nauk SSSR 66 (1949) 67.
[14] K.C. Hong, O.J. Kleppa, J. Chem. Thermodyn. 8 (1) (1976) 31–36.
[15] Z.A. Mateiko, G.A. Bukhalova, Z. Neorg. Khim. 6 (7) (1961) 1727.
[16] D.V. Semenstsova, G.A. Bukhalova, Z. Neorg. Khim. 12 (6) (1967) 1645–1649.
[17] I. Kostenska, J. Vrbenska, M. Malinivsky, Chem. Zvesti 28 (4) (1974) 531–538.
[18] V.A. Gladushchenko, M.A. Zakharchenko, Z. Neorg. Khim. 11 (1966) 916.
[19] P. Chartrand, A.D. Pelton, Metall. Trans. 32A (2001) 1385–1396.
[20] C.J. Barton, L.M. Bratcher, J.P. Blakely, W.R. Grimes, Phase Diagram of Nuclear Reactor Materials, ORNL-2548, in: R.E. Thoma (Ed.), Oak Ridge National Laboratory, Oak Ridge, TN, 1959, pp. 29–30.
[21] S. Cantor, J. Phys. Chem. 65 (1961) 2208–2210.
[22] P.P. Fedotieff, W.P. Iljinskii, Z. Anorg. U. Allgem. Chem. 129 (1923) 101–107.
[23] G.A. Bukhalova, V.T. Berezhnaya, Z. Neorg. Khim. 4 (11) (1959) 2596.
[24] J.P.M. van der Meer, R.J.M. Konings, K. Hack, H.A.J. Oonk, Chem. Mater. 18 (2006) 510–517.
[25] G.A. Bukhalova, E.P. Babaeva, Russ. J. Inorg. Chem. 10 (1965) 1026.
[26] L.A. Khripin, Izv. Sibir. Otdel. Akad. Nauk SSSR, Ser Khim. Nauk 7 (1963) 107.
[27] R.E. Thoma, G.D. Brunton, R.A. Penneman, T.K. Keenan, Inorg. Chem. 9 (1970) 1096.
[28] A.I. Agulyanskii, V. Bessonova, Russ. J. Inorg. Chem. 27 (1982) 579.
[29] F. Abdoun, M. Gaune-Escard, G. Hatem, J. Phase Equilib. 18 (1997) 6.
[30] O. Beneš, J.P.M. van der Meer, R.J.M. Konings, Comput. Coupling Phase Diagrams Thermochem. 31 (2007) 209–216.
[31] F. Matthes, S. Holz, Z. Chem. 2 (1962) 22.
[32] T. Grande, Thesis, University of Trondheim, Norway, 1992.
[33] O. Beneš, R.J.M. Konings, Comput. Coupling Phase Diagrams Thermochem. 32 (2008) 121–128.
[34] J.L. Holm, Acta Chem. Scand. 19 (1965) 638.
[35] G.A. Bukhalova, V.T. Berezhnaya, Russ. J. Inorg. Chem. 5 (2) (1959) 218–223.